High-Saturation High-Speed Traveling-Wave InGaAsP–InP Electroabsorption Modulator

G. L. Li, *Member, IEEE*, S. A. Pappert, P. Mages, C. K. Sun, W. S. C. Chang, and P. K. L. Yu

***Abstract*—High-saturation power traveling-wave electroabsorption modulators (TW-EAMs) with modulation bandwidth greater than 40 GHz have been demonstrated. Microwave properties of the TW-EAM waveguide are extracted from the measured S-parameters using the equivalent circuit model in [4]. Excellent agreement is obtained between the predicted and the measured frequency responses.**

***Index Terms*—Broad-band modulation, electroabsorption, high saturation, traveling-wave modulator.**

TRAVELING-WAVE electroabsorption modulators (TW-EAMs) can provide high-speed and high-efficiency features desirable for analog and digital fiber-optic links [1]–[5]. The major design concerns for the TW-EAM have been its low microwave waveguide impedance, slow microwave velocit, and large frequency-dependent microwave attenuation. In a previous work [4], we have established a comprehensive theoretical approach for analyzing the TW-EAM frequency response, including effects of impedance mismatch, velocity mismatch, and microwave attenuation. In [4], a distributed equivalent RF circuit model had been developed for representing the TW-EAM waveguide, with several practical approaches proposed for realizing a high efficiency TW-EAM with wide bandwidth.

In this letter, we demonstrate a broad-band TW-EAM using the low-impedance-termination approach. High slope efficiency and high optical saturation power have been achieved for fabricated devices. Also, excellent agreement is obtained between the measured frequency response and that predicted from traveling wave analysis. The modulation bandwidth is more than 40 GHz, and is limited by the bandwidth of equipment.

The TW-EAM employs the Franz–Keldysh effect in InGaAsP, with the p-type-intrinsic-n-type (p-i-n) layers grown on semi-insulating InP. In our design of the TW-EAM optical waveguide, particular attention is paid to the modulation efficiency. The material structure, in terms of layer thickness and composition, is optimized with respect to both the modulator slope efficiency and the coupling between the optical waveguide and the fiber [5]. The intrinsic InGaAsP layer, with background doping below 10^{16} cm^{-3}, has a bandgap of 1 eV and a thickness of 0.35 μm, and is sandwiched between two $\sim$1 μm-thick doped InGaAsP (1.08-eV bandgap) layers to form a large optical cavity. The doping concentration is around 2×10^{18} cm^{-3} for n-type layers, and graded from 5×10^{17} to 2×10^{18} cm^{-3} for p-type layers. To further facilitate the coupling to tapered fibers with 3-μm (diameter) spot size, the optical waveguide width is chosen to be 3 μm. The length of the electrode ranges from 150 to 300 μm. Vertical smooth sidewalls of the mesa have been achieved through wet chemical etching. Fig. 1 shows the schematic top view of the TW-EAM. The 50-Ω coplanar waveguide (CPW) microwave connection transmission lines on semi-insulating InP are made at the source and the termination ports to connect to microwave probes. Ground electrodes are connected via the n-layer and metal connections on top of the polyimide (see Fig. 1). The center electrodes of the CPWs are connected to the p-electrode of the modulator via polyimide bridges.

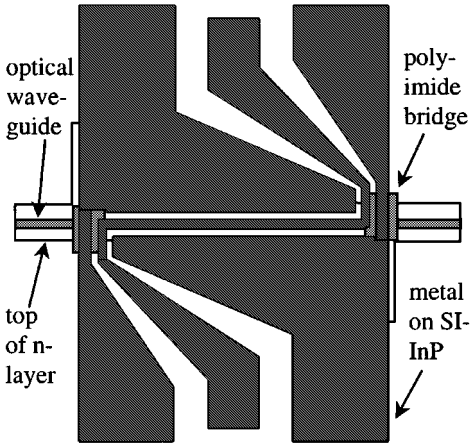

Fig. 1. Schematic top view of the TW-EAM showing the microwave electrodes and the optical waveguide.

The TW-EAMs show good DC characteristics. For a device with 200-μm-long electrode length plus 100-μm-long passive waveguide (caused by uncertainties in cleavage positions), the fiber-to-fiber optical insertion loss at zero bias has been measured to be 11.3 dB (at 1.32-μm wavelength). From the normalized transfer curve of this device, a slope efficiency of 0.65 V^{-1} has been obtained at –0.8 V bias. The slope efficiency can be enhanced if multiple quantum-well (MQW) absorption layer is used.

For the electrode structure shown in Fig. 1, the device can be considered as a two-port microwave device. A 40-GHz network analyzer (HP8510B) has been used to measure the two-port S-parameters for TW-EAMs with different electrode lengths. The microwave probes at both ports has been first calibrated out

Manuscript received January 23, 2001; revised May 7, 2001. This work was supported by Air Force Research Laboratory, by the Office of Naval Research, and by Raytheon under the Microelectronics Innovation and Computer Research Opportunity Program of California.

G. L. Li, P. Mages, W. S. C. Chang, and P. K. L. Yu are with the Department of Electronics and Computer Engineering, University of California, San Diego, La Jolla, CA 92093-0407 USA.

S. A. Pappert and C. K. Sun are with the SPAWAR Systems Center, San Diego, CA 92152-5001 USA.

Publisher Item Identifier S 1041-1135(01)08196-4.

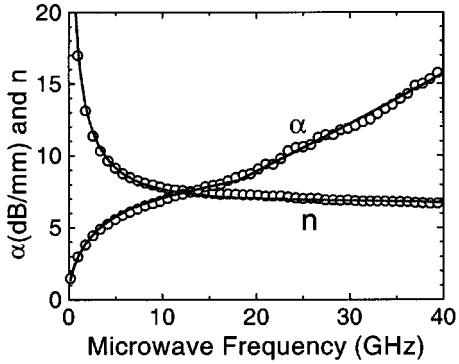

Fig. 2. Microwave attenuation factor and phase velocity index of TW-EAM waveguide. Symbols represent values extracted from measured S-parameters; solid lines are best fittings using the equivalent circuit model in [4].

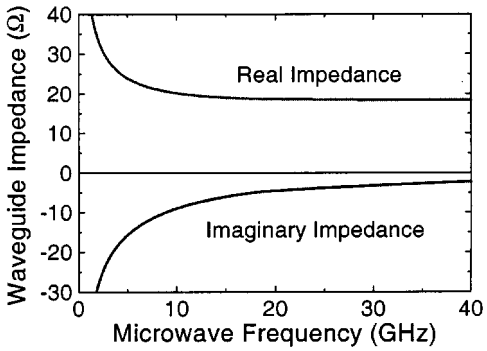

Fig. 3. Waveguide impedance calculated from equivalent circuit model for the fabricated TW-EAM.

in a standard full two-port calibration process. The microwave propagation constant $\gamma\,(=\alpha+j\beta)$ for the waveguide is then extracted using the ABCD transmission matrix approach [6]. The resulting microwave attenuation factor α and microwave phase velocity index $n\,(=\beta c/\omega)$ are plotted in Fig. 2.

Using the quasi-static equivalent circuit model in [4], the following circuit parameters for a unit length of TW-EAM microwave transmission line are derived by best fitting the α and n values, as shown by the solid lines in Fig. 2: the inductance $L_{\rm m} = 0.40$ nH/mm; the conduction resistance $R_{\rm con} = 7.3\ \Omega\text{-mm}^{-1}\ \text{GHz}^{-1/2}$; the device series resistance $R_{\rm S} = 0.58\ \Omega$-mm; and the junction capacitance $C_{\rm m} = 1.3$ pF/mm. Due to the finite gold thickness ($\sim$0.6 μm) on top of the waveguide, $R_{\rm con}$ is assumed to be a constant at frequencies below 18 GHz (i.e., $R_{\rm con} = 7.3{*}18^{1/2}\ \Omega$/mm). Above 18 GHz, $R_{\rm con}$ is proportional to the square root of frequency. To represent the dependence of the modulator current on the junction voltage, a $R_{\rm O}$ in parallel with $C_{\rm m}$ is used to designate the equivalent ac resistance due to the averaged optical absorption. Fig. 3 depicts the calculated TW-EAM microwave waveguide impedance at zero optical input using the above circuit parameters.

After the microwave properties of the p-i-n waveguide have been obtained, the microwave parameters of the connection CPW transmission lines on top of the semi-insulating InP substrate can be deduced. These transmission lines at both source and termination ports are included in calculating the TW-EAM modulation frequency response using the analysis

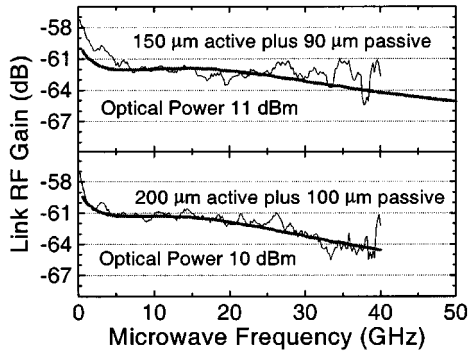

Fig. 4. Measured (thin noisy lines) and calculated (thick smooth lines) frequency responses for two TW-EAM devices. The detector responsivity is $\sim$ 0.12 A/W up to 40 GHz.

in [4]. In the same equivalent circuit model, $R_{\rm O}$ at a given optical input level can be estimated from the slope of the electroabsorption modulator (EAM) dc photocurrent versus voltage curves ($R_{\rm O} \sim$300 Ω-mm at 10-dBm input optical power).

For the frequency response measurement, the termination port of the TW-EAM devices is contacted by a 50-GHz microwave probe that provides a termination impedance of 26.2 Ω. It is found that the frequency response curves show a low frequency rolloff due to the passive optical waveguide. This is mainly due to the absence of metal on top of the passive waveguide, so that the microwave loss in the passive waveguide increases much faster with frequency. For example, for a device with 150-μm-long electrode length and 90-μm-long passive waveguide, the effective modulation length is $\sim$240 μm for frequencies below $\sim$0.2 GHz and 150 μm for frequencies above 5 GHz. This modulation length change gives rise to the apparent low frequency rolloff $(20{*}\log{(240/150)} = 4.1$ dB). The low frequency rolloff characteristic can be eliminated by more accurate cleaving.

The measured frequency response for TW-EAM devices (with the passive waveguide) including the photodetector conversion loss is shown in Fig. 4. The microwave probe at the source port has been calibrated out. For the 150-μm-long device, the 3-dB modulation bandwidth is larger than 40 GHz. For the 200-μm-long device, the bandwidth is measured at $\sim$35 GHz. The calculated TW-EAM frequency responses are also plotted in Fig. 4. The calculated curves fit the measured curves very well, and a 50-GHz modulation bandwidth is predicted for the 150-μm-long device.

Link RF gain using 200-μm-long TW-EAM devices (terminated with 26.2 Ω) is measured against input optical power, with microwave frequency fixed at 18 GHz and detector responsivity of 0.6 A/W. The results are plotted in Fig. 5. The top curve is for a device biased at -0.8 V with transfer curve slope efficiency of $0.65\ \text{V}^{-1}$; while the bottom curve is for another device biased at -1.3 V with the slope efficiency of $0.47\ \text{V}^{-1}$. The optical saturation power at 1-dB RF gain compression point is 25 mW for the first device and 45 mW for the second device. The difference of the saturation power for these two devices is mainly caused by the 0.5-V bias difference. Comparing with lumped element EAM possessing the same large bandwidth, TW-EAM has longer waveguide length, so that its optical absorption is more distributed. This leads to the higher saturation power of

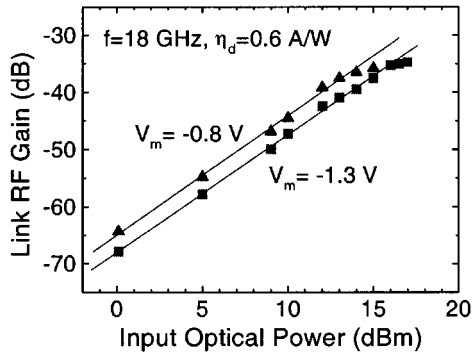

Fig. 5. High-frequency optical saturation power for two 200-μm-long TW-EAMs with 100-μm-long passive waveguide.

TW-EAM. The high saturation power of our TW-EAM devices is also contributed by the design of layer structure with graded band-offset, so that the hole-piling effect is reduced. At the photodetector responsivity of 0.6 A/W, the maximum RF gain is about -35 dB for both of the above TW-EAM devices. AR coating and more accurate cleaving can improve the RF link gain.

In summary, wide bandwidth and high efficiency InGaAsP–InP TW-EAM devices have been designed and fabricated according to our previously proposed low-impedance-termination approach. Improvement in modulation efficiency can be obtained by using MQW material in the modulation layer. The results indicate that the traveling-wave EAM design is a very promising and practical approach for broad-band millimeter wave, as well as high-speed communication applications.

REFERENCES

[1] H. H. Liao, X. B. Mei, K. K. Loi, C. W. Tu, P. M. Asbeck, and W. S. C. Chang, "Microwave structures for traveling-wave MQW electro-absorption modulators for wide band 1.3 μm photonic links," in *Proc. SPIE, Optoelectron. Integrated Circuits*, vol. 3006, 1997, pp. 291–300.

[2] K. Kawano, M. Kohtoku, M. Ueki, T. Ito, S. Kondoh, Y. Noguchi, and Y. Hasumi, "Polarization-insensitive traveling-wave electrode electroabsorption (TW-EA) modulator with bandwidth over 50 GHz and driving voltage less than 2 V," *Electron. Lett.*, vol. 33, pp. 1580–1581, 1997.

[3] S. Z. Zhang, Y. J. Chiu, P. Abraham, and J. E. Bowers, "25-GHz Polarization-insensitive electroabsorption modulators with traveling-wave electrodes," *IEEE Photon. Technol. Lett.*, vol. 11, pp. 191–193, Feb. 1999.

[4] G. L. Li, C. K. Sun, S. A. Pappert, W. X. Chen, and P. K. L. Yu, "Ultra high-speed traveling wave electroabsorption modulator: Design and analysis," *IEEE Trans. Microwave Theory Tech.*, vol. 47, pp. 1177–1183, 1999.

[5] G. L. Li, D. S. Shin, W. S. Chang, P. M. Asbeck, P. K. L. Yu, C. K. Sun, S. A. Pappert, and R. Nguyen, "Design and fabrication of traveling wave electroabsorption modulator," in *Proc SPIE, Optoelectron. Integrated Circuits IV*, vol. 3950, 2000, pp. 252–255.

[6] D. M. Pozar, *Microwave Engineering*. Reading, MA: Addison-Wesley, 1990, pp. 231–235.